AD-A189 478

②

AFWAL-TR-87-3081

SUPERSONIC, TRANSVERSE JET FROM A ROTATING OGIVE CYLINDER

IN A HYPERSONIC FLOW

Daniel L. McMaster
Universal Energy Systems
4401 Dayton-Xenia Road
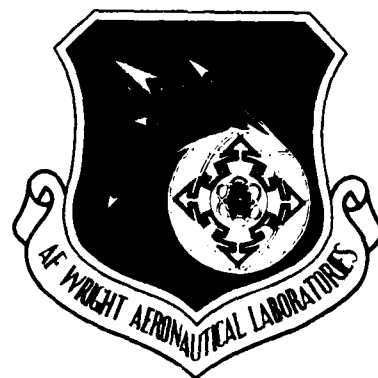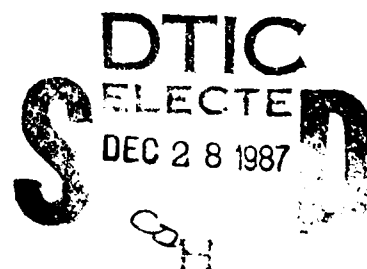Dayton OH 45432

NOVEMBER 1987

DTIC
ELECTE
DEC 2 8 1987

FINAL REPORT FOR JANUARY – SEPTEMBER 1987
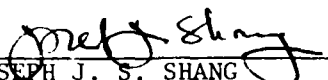
Approved for public release; distribution unlimited.

87 12 16 065

NOTICE

When Government drawings, specifications, or other data are used for any purpose other than in connection with a definitely Government-related procurement, the United States Government incurs no responsibility or any obligation whatsoever. The fact that the Government may have formulated or in any way supplied the said drawings, specifications, or other data, is not to be regarded by implication, or otherwise in any manner construed, as licensing the holder, or any other person or corporation; or as conveying any rights or permission to manufacture, use, or sell any patented invention that may in any way be related thereto.
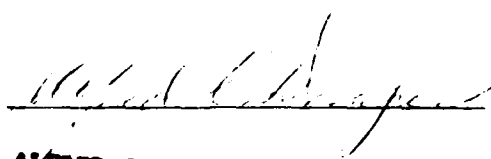
This report has been reviewed by the Office of Public Affairs (ASD/PA) and is releasable to the National Technical Information Service (NTIS). At NTIS, it will be available to the general public, including foreign nations.

This technical report has been reviewed and is approved for publication.

JOSEPH J. S. SHANG
Technical Manager
Computational Aerodynamics Group

BOHDAN G. KUNCIW, Maj, USAF
Chief, Aerodynamics and Airframe Br.
Aeromechanics Division

FOR THE COMMANDER

ALFRED C. DRAPER
Acting Chief
Aeromechanics Division

REPORT DOCUMENTATION PAGE

Form Approved
OMB No. 0704-0188

1a. REPORT SECURITY CLASSIFICATION	1b. RESTRICTIVE MARKINGS
UNCLASSIFIED	

2a. SECURITY CLASSIFICATION AUTHORITY	3. DISTRIBUTION/AVAILABILITY OF REPORT
	Approved for public release; distribution is unlimited.
2b. DECLASSIFICATION/DOWNGRADING SCHEDULE	

4. PERFORMING ORGANIZATION REPORT NUMBER(S)	5. MONITORING ORGANIZATION REPORT NUMBER(S)
	AFWAL-TR-87-3081

6a. NAME OF PERFORMING ORGANIZATION	6b. OFFICE SYMBOL (If applicable)	7a. NAME OF MONITORING ORGANIZATION
Universal Energy Systems (UES)		Flight Dynamics Laboratory (AFWAL/FIMM) Air Force Wright Aeronautical Laboratories

6c. ADDRESS (City, State, and ZIP Code)	7b. ADDRESS (City, State, and ZIP Code)
4401 Dayton-Xenia Road Dayton OH 45432	Wright-Patterson AFB OH 45433-6553

8a. NAME OF FUNDING/SPONSORING ORGANIZATION	8b. OFFICE SYMBOL (If applicable)	9. PROCUREMENT INSTRUMENT IDENTIFICATION NUMBER
		F33615-86-C-3800

8c. ADDRESS (City, State, and ZIP Code)	10. SOURCE OF FUNDING NUMBERS

PROGRAM ELEMENT NO.	PROJECT NO.	TASK NO.	WORK UNIT ACCESSION NO.
61102F	2307	N6	11

11. TITLE (Include Security Classification)

Supersonic, Transverse Jet from a Rotating Ogive Cylinder in a Hypersonic Flow

12. PERSONAL AUTHOR(S)
D. L. McMaster

13a. TYPE OF REPORT	13b. TIME COVERED	14. DATE OF REPORT (Year, Month, Day)	15. PAGE COUNT
Final Report	FROM Jan 87 TO Sep 87	NOVEMBER 1987	48

16. SUPPLEMENTARY NOTATION

17. COSATI CODES			18. SUBJECT TERMS (Continue on reverse if necessary and identify by block number)
FIELD	GROUP	SUB-GROUP	
01	01		
01	03		

19. ABSTRACT (Continue on reverse if necessary and identify by block number)
Numerical simulations were performed for a supersonic jet issuing from a blunt-nosed ogive cylinder into a Mach 12 cross stream. All calculations employed the finite differenced, mass-averaged Navier-Stokes equations with an algebraic eddy viscosity model for turbulence closure. One portion of the present investigation was focused on the numerical resolution requirement for the three-dimensional separated flow field around the non-rotating body. For this purpose, four solutions were obtained using mesh systems with different numbers of grid points and clustering. The secondary separated flow field structure was resolved with moderately increased grid density. The major portion of the present study was devoted to the simulation of the flow field around the identical configuration with the added complexity of rotating motion about the principal axis of the body. Numerical solutions over a wide range of angular velocities were obtained in the rotating frame of reference. The effects of rotation on the global flow field structure and especially the jet plume formation were examined through a comparative study from the viewpoint of a stationary observer. At the low angular velocity of interest, the effects of body rotation on the flow field structure were insignificant.

20. DISTRIBUTION/AVAILABILITY OF ABSTRACT	21. ABSTRACT SECURITY CLASSIFICATION
☒ UNCLASSIFIED/UNLIMITED ☐ SAME AS RPT ☐ DTIC USERS	UNCLASSIFIED

22a. NAME OF RESPONSIBLE INDIVIDUAL	22b. TELEPHONE (Include Area Code)	22c. OFFICE SYMBOL
Joseph J. S. Shang	(513) 255-7127	AFWAL/FIMM

DD Form 1473, JUN 86   Previous editions are obsolete

ACKNOWLEDGEMENT

iii

TABLE OF CONTENTS

LIST OF FIGURES

SECTION I

INTRODUCTION

The interaction of a transverse jet with an oncoming stream is a fundamental and important aerodynamic phenomenon in many flow regimes. In the subsonic domain, examples include the discharge of gases from smokestacks, mixing and combustion, and VTOL/STOL technology. For supersonic flows, the characteristics of the transverse jet interaction are important to control and maneuverability of aerospace vehicles as well as supersonic combustion. However, our knowledge of this complex physical phenomenon is still very limited and urgently needs continued research efforts.

Investigators have considered many aspects of the interacting transverse jet problem, including jet dynamics (References 1-9), entrainment and mixing (References 1-3, 6, 10), induced pressure distributions (References 8, 11, 12), shock interaction (References 8, 11, 13-15), and numerical solutions (References 5-7, 13, 16). Few investigators have attempted to calculate the complete three-dimensional flow field. Even fewer have attempted numerical simulations utilizing the ensembled compressible Navier-Stokes equations. None, to our knowledge, have studied the nature of the flow field when the jet-issuing body is rotating with respect to its principal axis.

For the case of a supersonic primary stream and a non-rotating body, the flow field is characterized by the

1

inviscid-viscous interaction similar to that induced by a protuberance (References 17, 18). Complex patterns of shock interaction together with three-dimensional vortical structures are created as the flow is diverted around the jet. The phenomenon of interference which forms separation regions is well documented for many types of flow field obstructions (References 17, 18). In the case of a jet in a hypersonic primary stream, the domain of influence is significantly reduced. Therefore, the gradients of flow properties are much steeper and the scales of the resultant flow structures are changed. The three-dimensional separated flow must, however, obey topological rules which maintain the continuity of the flow field (References 17, 19-21). In order to capture the detailed flow field structure, a large amount of computer resources is required. When the jet issuing body rotates about its longitudinal axis, there is no plane of symmetry to reduce the computational domain, and the grid resolution problem becomes more severe. The first portion of the present study establishes the criterion for numerical resolution of the three-dimensional interaction which is generated by a supersonic jet issuing from a blunt-nosed ogive cylinder into a hypersonic stream.

The major portion of the present study concerns the calculation and correlation of the flow field past the jet issuing cylinder rotating about its longitudinal axis under identical test conditions. The numerical simulation is not dynamically coupled; the ogive cylinder is assumed to remain at zero angle

of attack at all times. Two approaches are possible in describing the rotational fluid motion. The first method is to define the coordinates in the Newtonian frame and generate the instantaneous grid system according to the motion. The other approach is to describe the fluid motion in the rotating frame of Reference 22. This latter approach is more suitable to our present purpose. First, calculation in the rotating frame of reference is simpler because the grid need not be rotated at each time step. Second, since the deformation tensor is invariant under rotational transformation, calculation in the rotating frame of reference still allows us to determine viscous effects (such as the shear flow pattern) while maintaining an easily implemented computer code. Finally, the additional acceleration due to the non-rectilinear motion can be singled out easily to assess the impact on the complete flow field. Once the flow field is obtained in the moving frame of reference, the results are compared to the non-rotating results to exhibit the change in the flow field appearance from the viewpoint of a stationary observer. Of particular interest are (1) the global flow structure affected by the rotating motion, and (2) the flow field properties in the jet plume.

SECTION II

GRID REFINEMENT STUDY

1. ANALYSIS

A side-by-side numerical and experimental study (Reference 13) of the entire flow field for a configuration consisting of a transverse jet issuing from a blunt-nosed ogive cylinder was recently accomplished. This solution will be designated as case A. Figure 1 compares the schlieren photograph of the flow interaction with computed density contours. The global features of the flow are captured by the computation, although there is a slight discrepancy in the projected angle of the bow shock envelope induced by the jet. Based on our experience, this is a first clear indication of insufficient numerical resolution for this complex physical phenomenon.

Figure 2 depicts the comparison of the experimental and computed pitot pressure profiles at three locations downstream of the jet. The shock structure can be determined, but as is common (References 13, 17, 23), the profile is smeared due to the lack of grid-point density in the high-gradient region. We feel that the flow field solution is still valid, but the shock smearing detracts from the value of the numerical simulation for this comparative study. Another poor agreement between computed and experimental results is seen near the wall, particularly at $\Delta X/D = 2$. We are reasonably certain that some of the disagreement is due to insufficient grid resolution, but this observed discrepancy may also be attributed to the

4

$M_\infty = 12.0$

$REY = 0.58 \times 10^6$

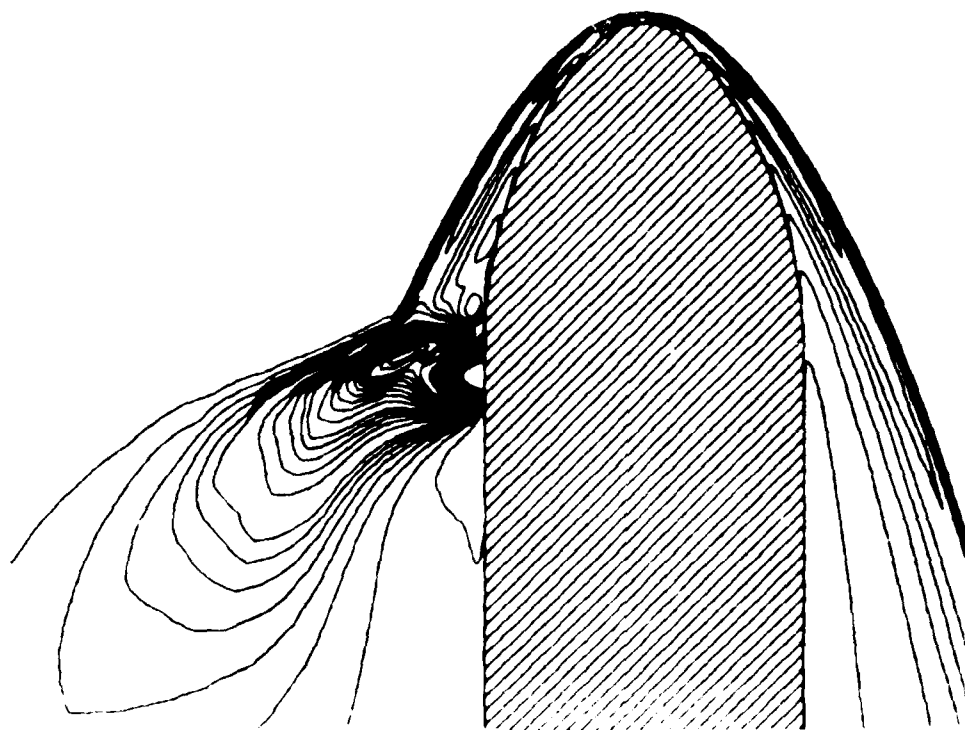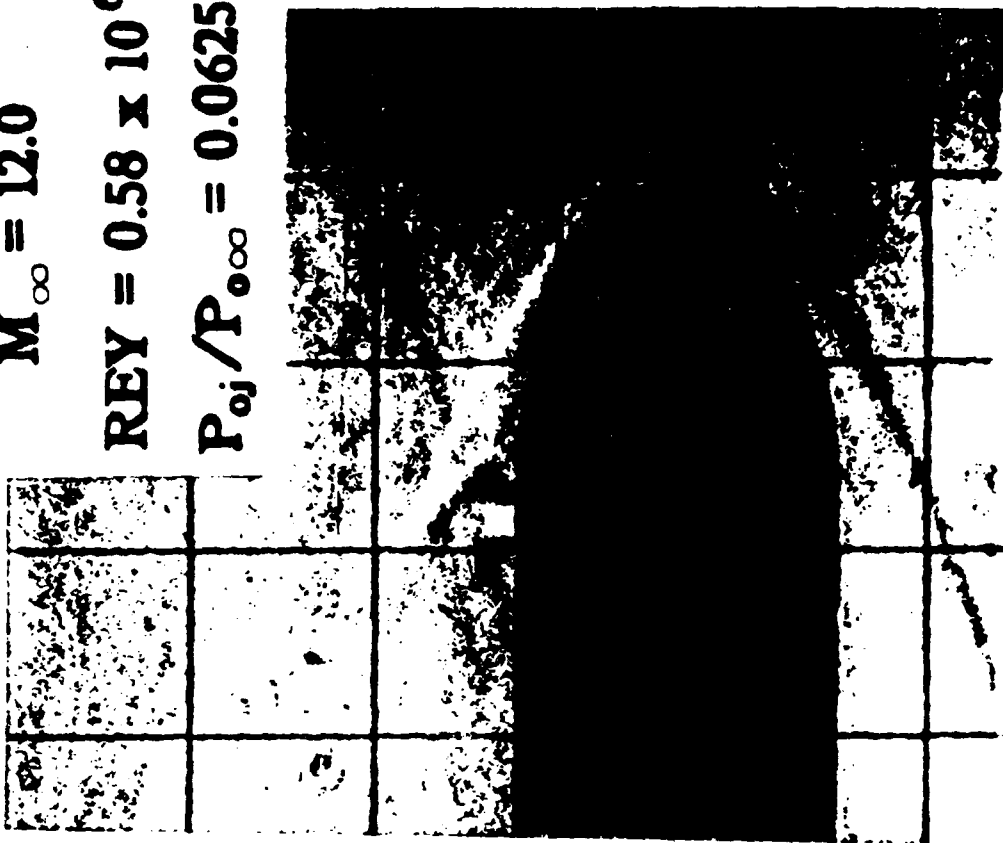$P_{oj}/P_{o\infty} = 0.0625$

Figure 1. Comparison of Schlieren Photograph
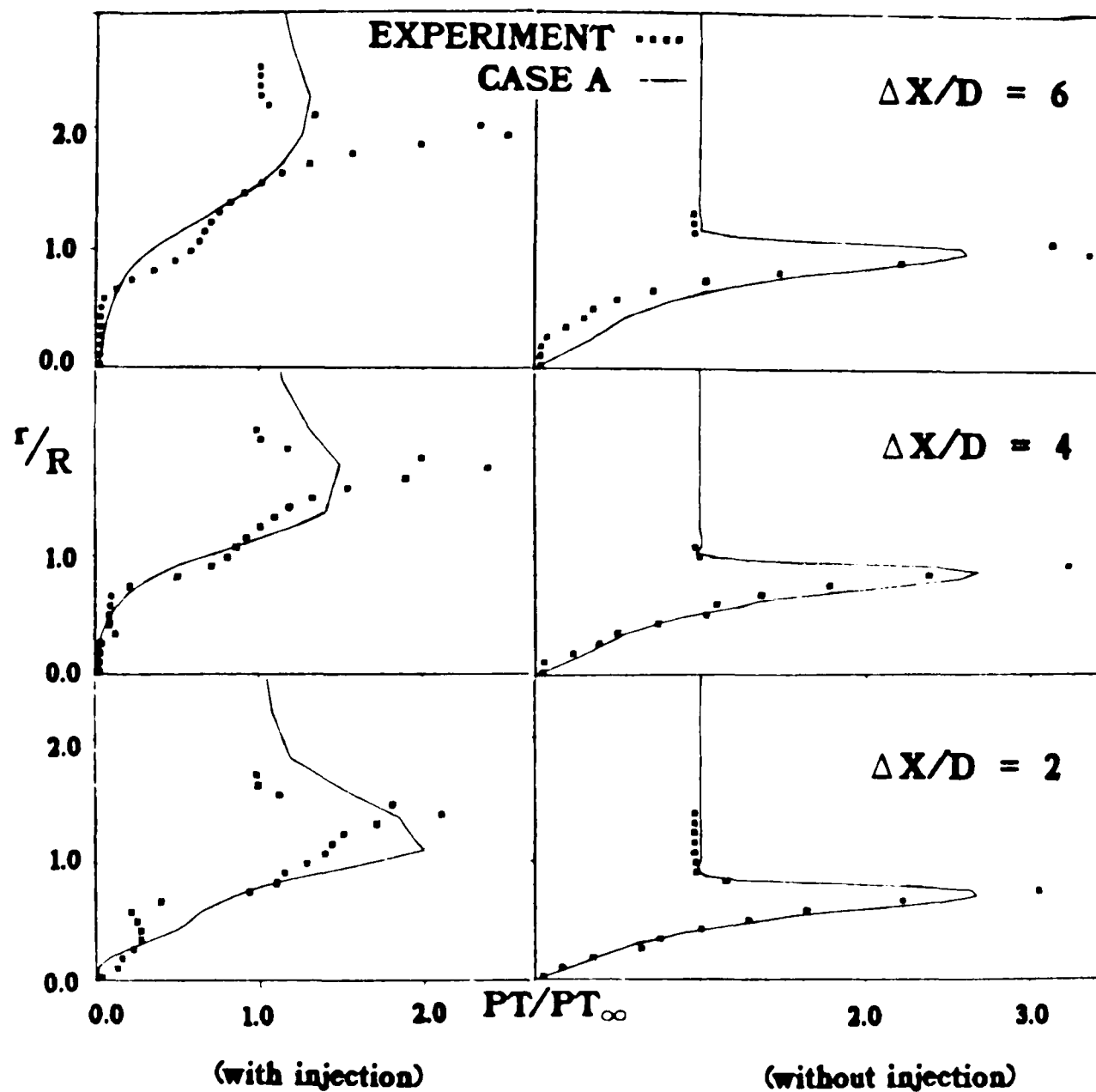with Density Contours for Case A

Figure 2. Comparison of Pitot Pressure Profile

6

combined effects of the inadequate turbulence modeling, and possible inaccuracies in the experimental data. The source of error in pitot pressure measurements might be traced to the fact that the pitot probe was aligned only in the freestream direction. In the region near the wall, the main flow direction is dictated by the jet interaction and mixing. The flow deflection to the unperturbed flow has reached a value as high as 45°. This particular issue of the data accuracy will remain open and unresolved in the present analysis.

As a final representation of the accuracy of the computed solution, we examine Figure 3, comparing the computed surface velocity vectors with photographic evidence from the experiment. Although the general agreement is reasonable, we can see a major topological discrepancy in the region upstream of the jet. The experimental oil pattern clearly shows two lines of convergence and two lines of divergence. The computed flow field has only one clear line of convergence, and one line of divergence. This qualitative disparity represents a more serious problem in numerically replicating three-dimensional, separated flows than does the previously described quantitative difference.

On the basis of the above observations, efforts were concentrated to determine the requisite grid refinement which was sufficient to negate the discrepancies noted between experimental and computational data. Particular emphasis was placed on the resolution of the separated flow upstream of the jet to

CASE A
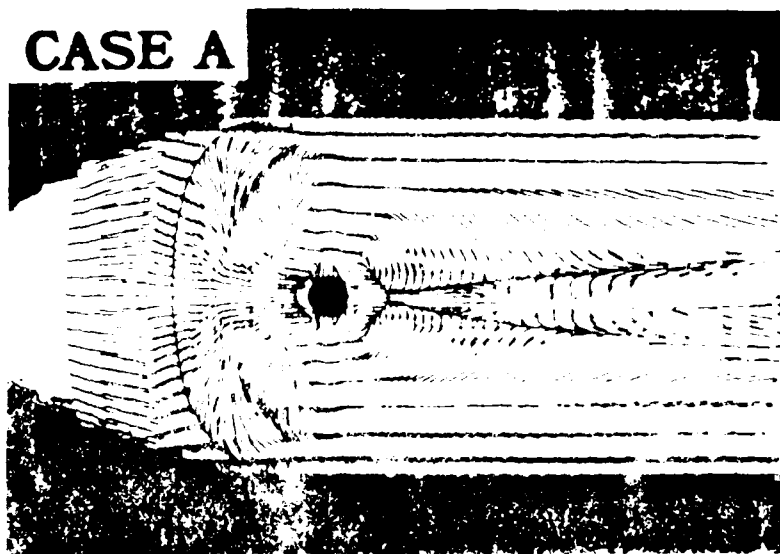
$M_\infty = 12.0$

EXPERIMENT
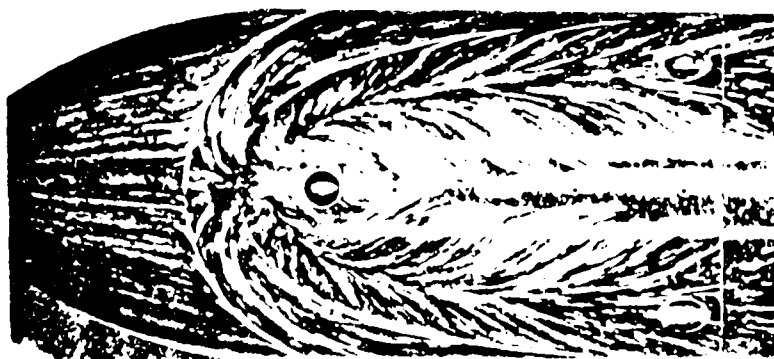
$REY = 0.58 \times 10^6$

$P_{oj}/P_{o\infty} = 0.0625$

Figure 3. Comparison of Shear Flow Patterns

achieve a grid invariant numerical solution. In the grid refinement process, we constructed the grid system by clustering grid points around the anticipated resultant shock wave envelope but without the explicit use of automated grid adaptation.

Four grids, designated grids A-D, were used for the resolution study. Side views of each grid are presented in Figure 4. All grids had two regions of clustering in the normal direction. Grid points were clustered near the body to resolve the boundary layer and away from the body to capture the bow shock wave. The most coarse grid system, used in the previous study to calculate case A, had 100 x 45 x 42 points in the streamwise, normal, and azimuthal directions, respectively. Grid B, which consisted of 120 x 50 x 50 grid points, was designed to resolve the existence and location of the possible secondary vortical structure upstream of the jet. The results of computations on this grid are designated as case B. The additional 20 streamwise planes are added in the region upstream of the jet. The streamwise spacing in this region is decreased by a factor of two over that of grid system A to Order $\delta/10$, where δ is the undisturbed boundary layer thickness computed at the jet location on the opposite side of the cylinder. The third grid, grid C, was generated in an attempt to capture the shock location downstream of the jet; it had 110 x 70 x 50 points, with the majority of the added points located downstream of the jet, between the body and the experimentally predicted shock location.
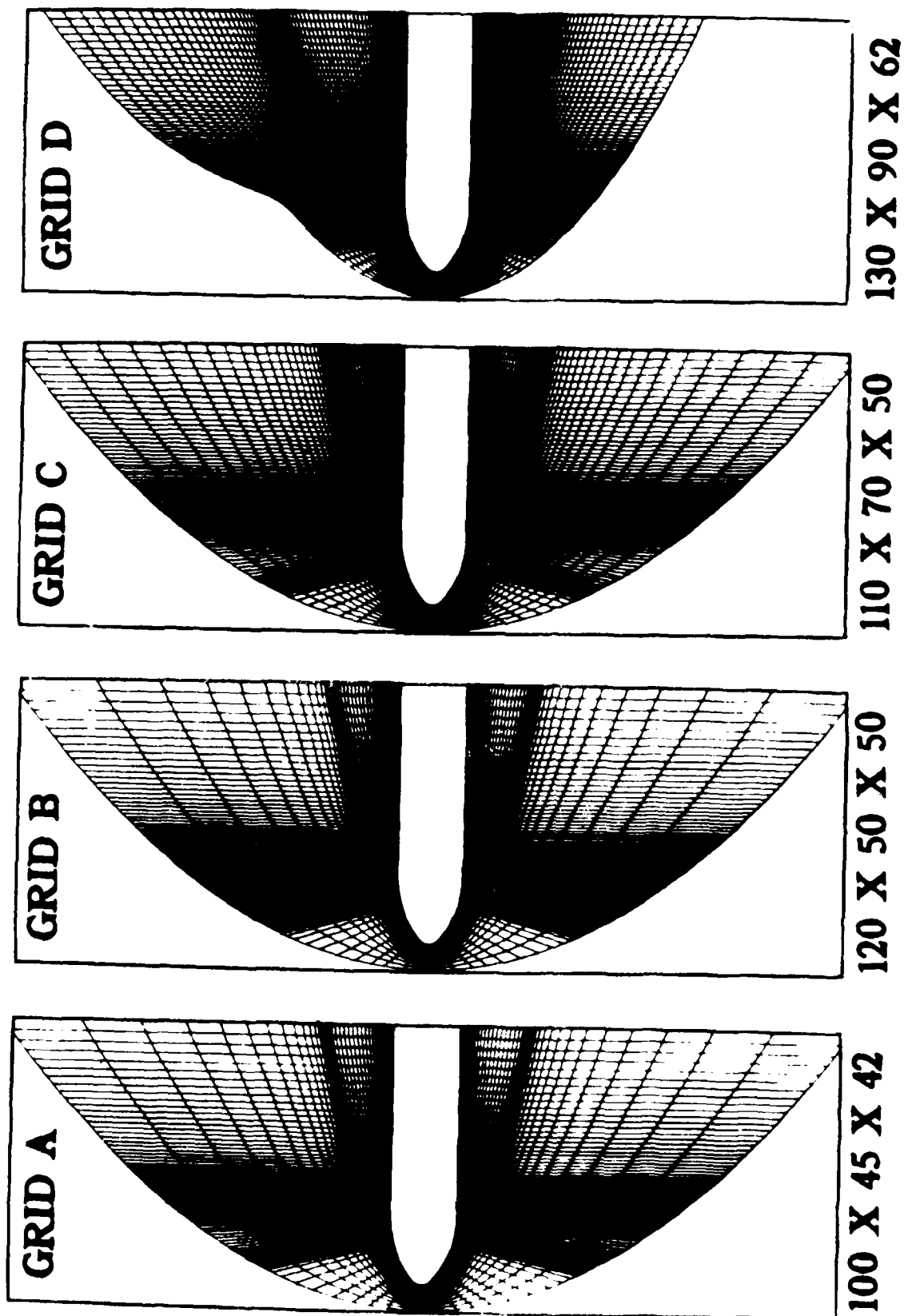
Figure 4. Side View of Grid Points in the Plane of Symmetry

GRID A
100 X 45 X 42

GRID B
120 X 50 X 50

GRID C
110 X 70 X 50

GRID D
130 X 90 X 62

A fourth grid, grid D, was a final attempt to resolve as many of the features of the flow field as possible in one grid system. Grid D represented increased spatial refinement over cases A, B, and C, both upstream and downstream of the jet. It was dimensioned 130 x 90 x 62, and was fitted to the general structure of the predicted shock wave envelope of jet interaction. The side view of this grid system shows that downstream of the jet, the grid clustering for the anticipated shock wave envelope moves away from the body. The grid expansion is limited to the jet-injection side of the body; the opposite side retains the same basic spacing as the grids in cases A-C.

Table 1 compares cases A-D for their relative grid size, using case A as the baseline. Since computational time required to reach convergence is proportional to the number of grid points, one can see that the increase in resource consumption is significant for all three grid enhancements.

The numerical solutions were obtained using the three-dimensional, mass-averaged Navier-Stokes equations with a

Table 1. RELATIVE GRID SIZES

Case	Dimensions	Relative Size[*]
A	100 x 45 x 42	1
B	120 x 50 x 50	1.59
C	110 x 70 x 50	2.04
D	130 x 90 x 62	3.84

[*]Relative Size = Number of Grid Points/Number of Grid Points for Case A.

simple flux-gradient turbulence model (Reference 24). The numerical procedure was based on MacCormack's explicit predictor-corrector algorithm (Reference 25), vectorized for high speed processors. The data processing rate was 4×10^{-5} seconds per grid point per iteration on the Cray 2 at NASA Ames Research Center. Local time stepping was used to speed convergence with the required convergence criterion that the consecutive surface pressure change less than one percent over a characteristic time scale.

2. DISCUSSION OF RESULTS

The comparison of computed pitot pressure profiles with increasing numerical resolution (cases A, C, and D) together with experimental data is given in Figure 5. In general, a steady improvement of shock wave definition was gained with higher grid point density and better distribution of mesh nodes near the experimentally predicted location of the shock. In particular, grid system D represented the most elaborate grid refinement and yielded the best agreement with data. The maximum deviation between experimental data and numerical results is persistently located at the wave front. Further refinement of the numerical results could be obtained by adding more grid points and by redistributing the mesh system at the expense of substantially more computer resources. The use of shock fitting and/or three-dimensional adaptive techniques might conceivably be even more effective in obtaining the desirable definition of the shock wave envelope. Finally, the influence
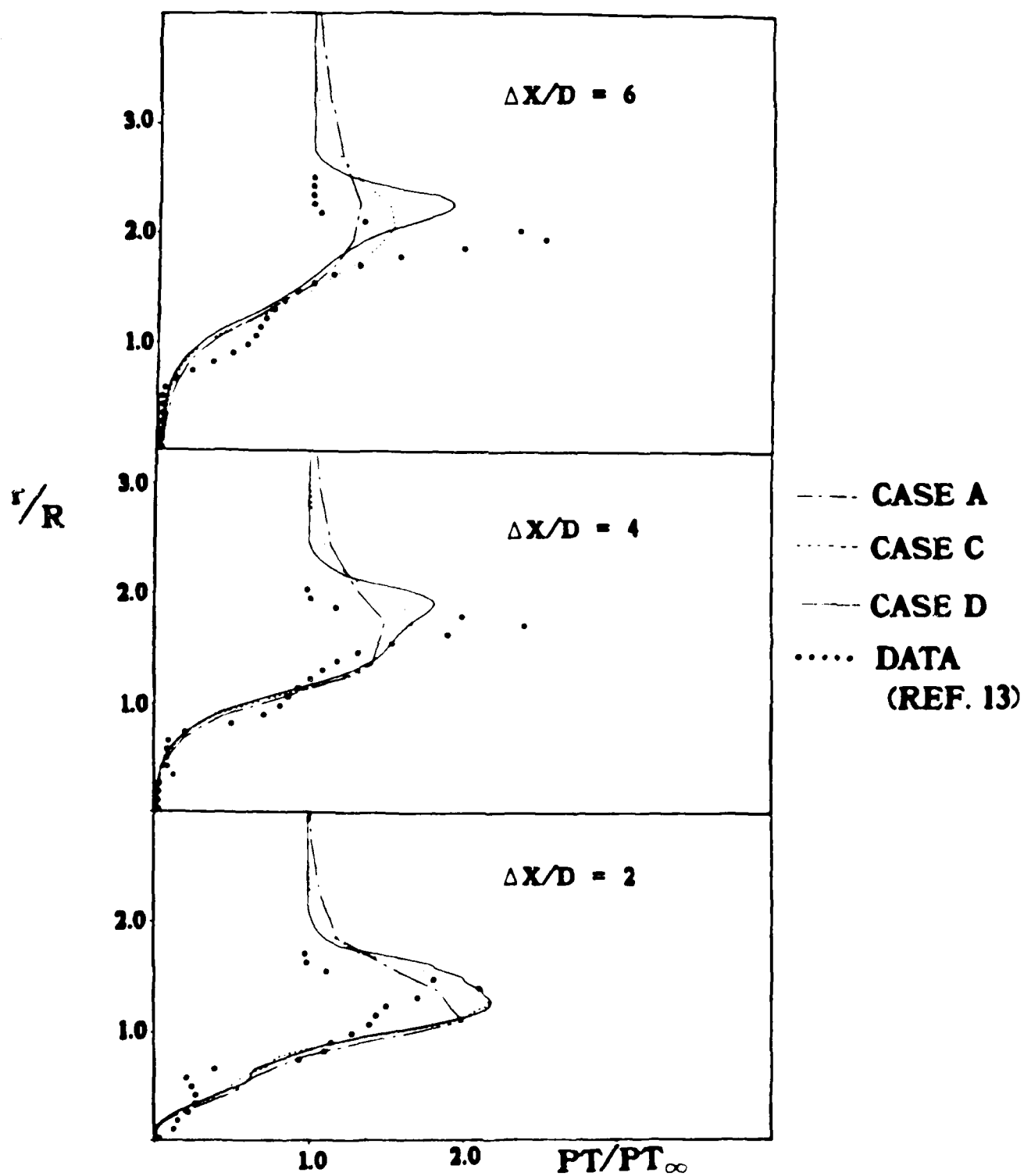
12

Figure 5. Comparison of Pitot Pressure Profiles

of the turbulence model on the numerical results was evaluated
by suppressing the numerical transition from laminar to turbu-
lent flow downstream of the jet, thereby restricting the
numerical simulation to laminar flow throughout the computa-
tional domain. This numerical result revealed a correct out-
ward displacement of the shock wave structure downstream of the
jet, but did not demonstrate any significant change in the
pitot pressure profile near the body surface.

The computed surface oil flow patterns are shown in Figure
6 for cases A and B. The two numerical results are markedly
different in that case B shows a distinct secondary convergence
line near the plane of symmetry, whereas no such line is
present in case A. The locations of the lines of convergence
and divergence are within the experimental error-band of
surface oil streaks under the identical flow conditions.

A side view of the vector field in the plane of symmetry
ahead of the jet for case B is shown in Figure 7. We can
clearly detect the small secondary reversed flow region adja-
cent to the body surface. The greatest dimension associated
with the secondary structure is less than the boundary layer
thickness of the unperturbed stream. The presence of the
secondary separation region affected the global flow field
construct negligibly. This can be seen from Figure 8, which
compares the plane of symmetry density contours for cases A and
B. One may conclude that the increase in resolution for case B
does increase the accuracy of the description of the separated

CASE A
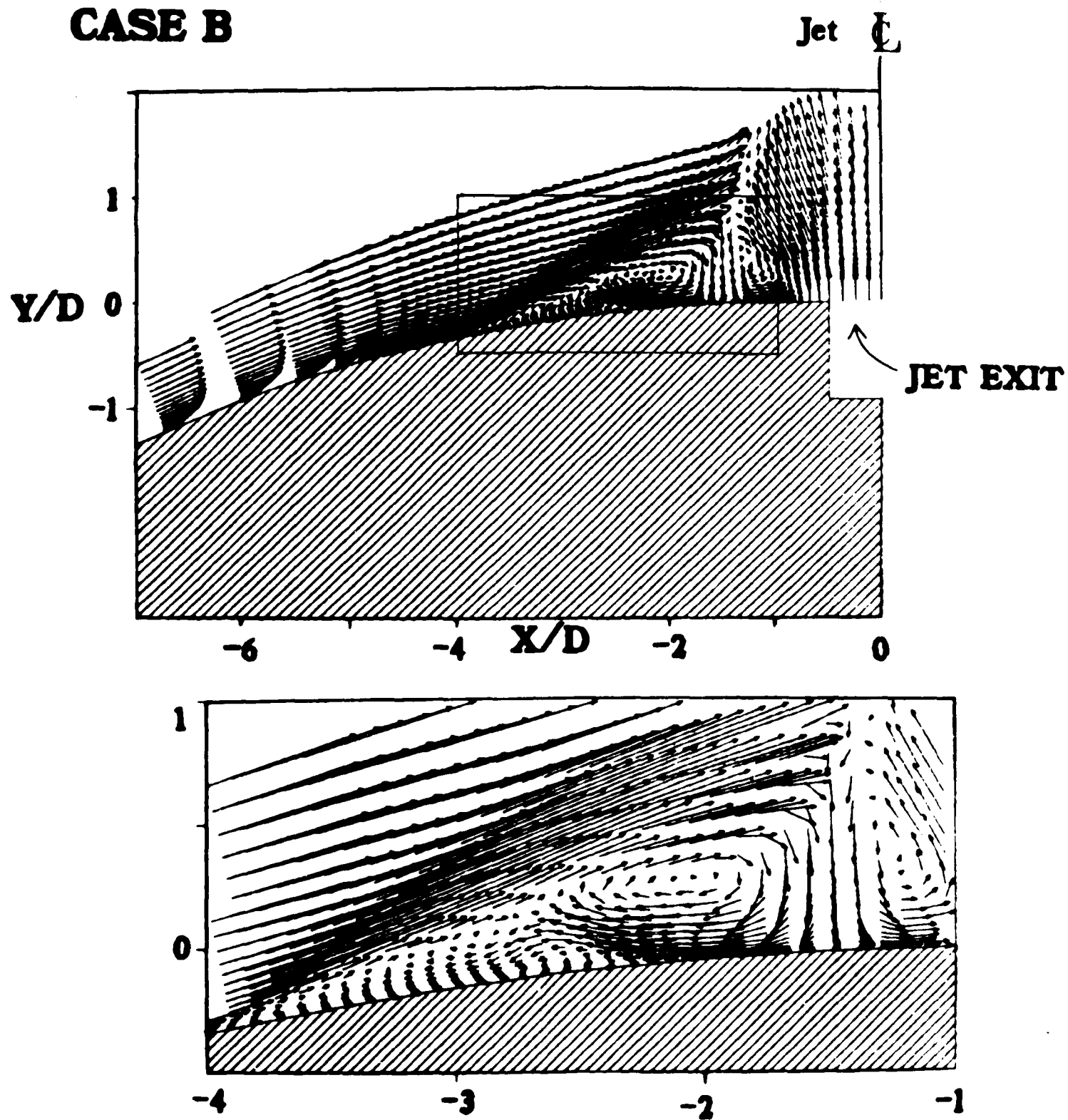
CASE B

CASE B

Jet ₵
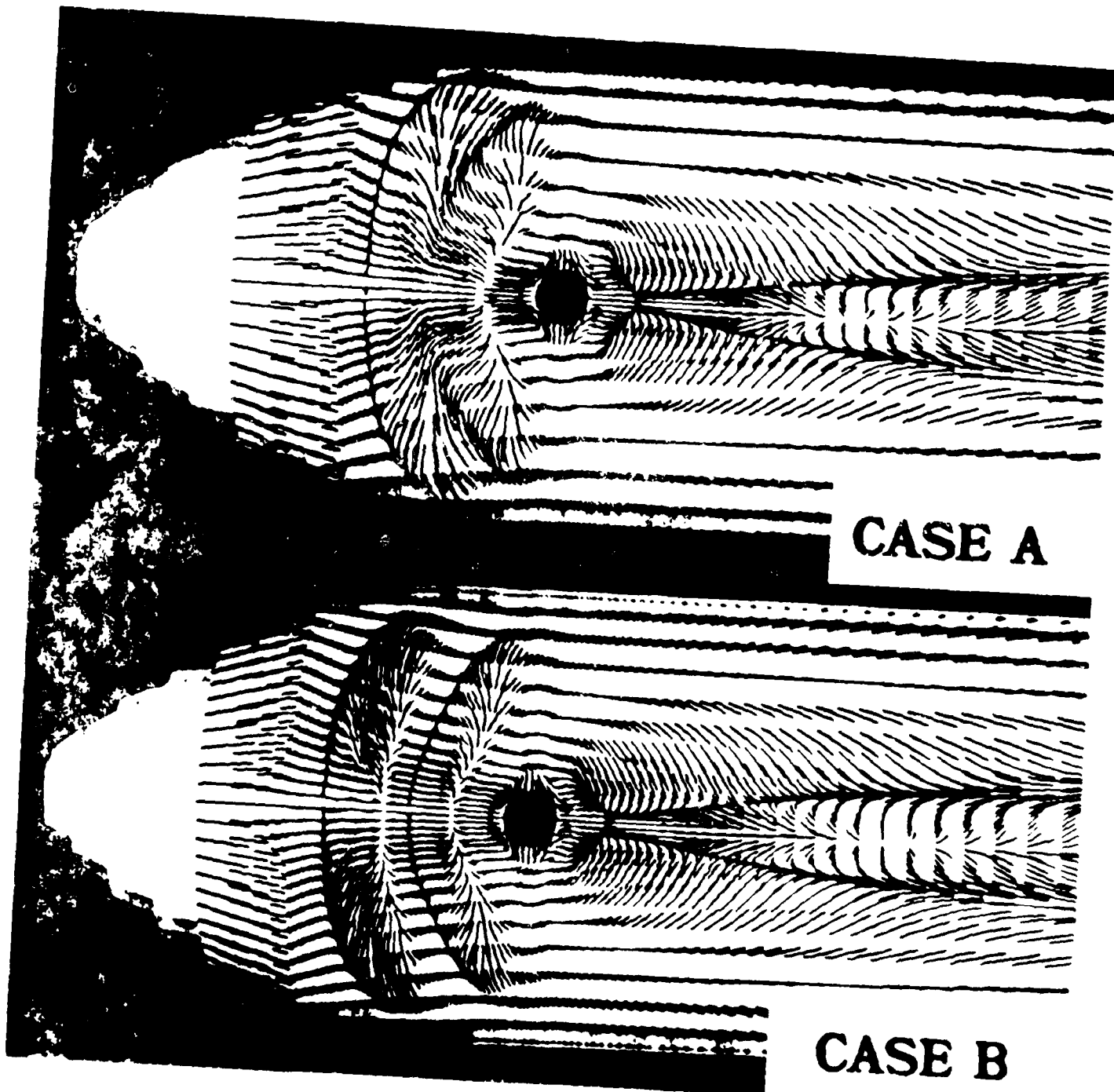
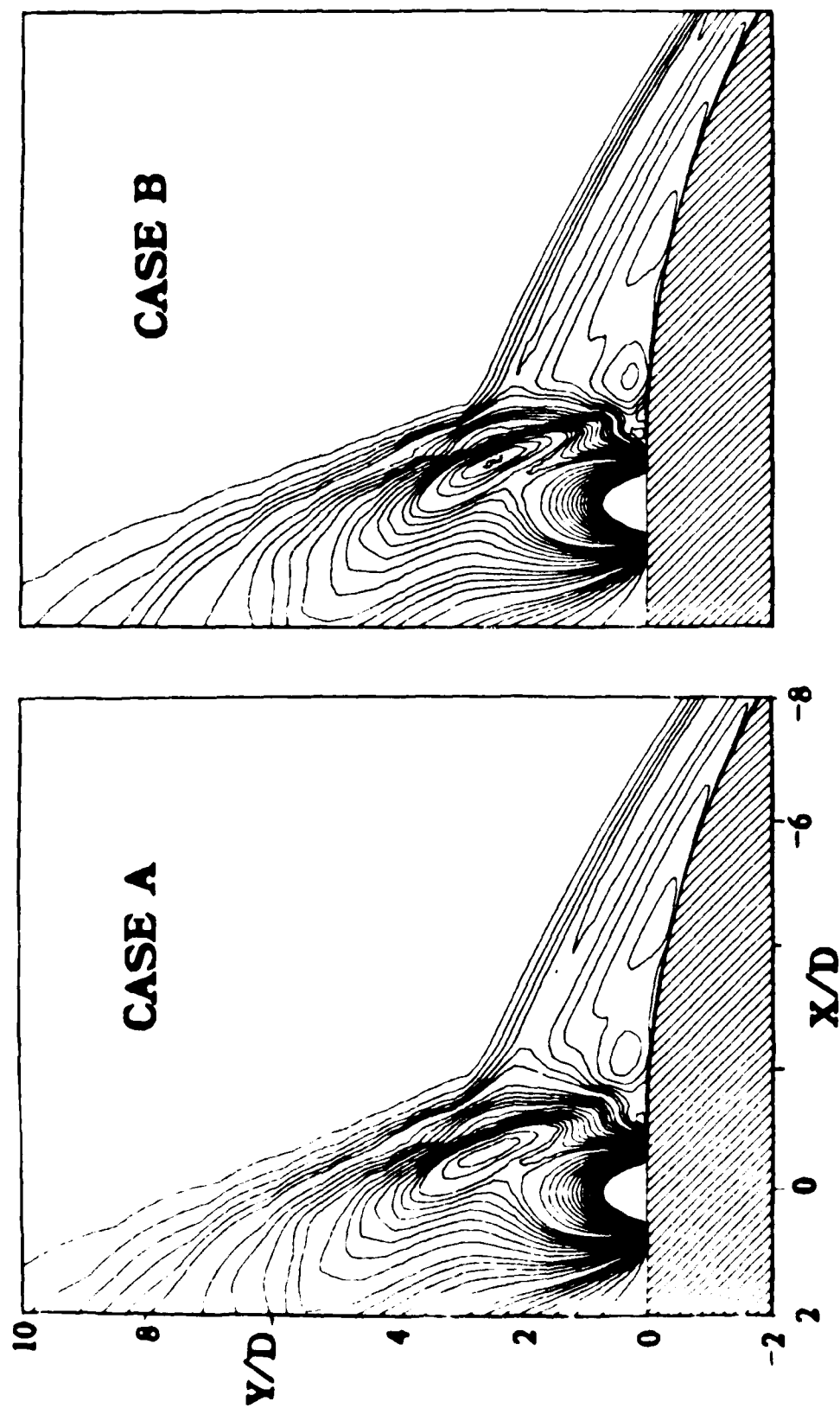
Figure 7. Velocity Vectors in the Plane of Symmetry

Figure 8. Closeup Comparison of Density Contours
in the Plane of Symmetry

flow field. The predicted secondary vortical structure is found to replicate experimental observations. The secondary vortical structure influence is local, so that the relatively sparse resolution upstream of the jet is not overly critical in capturing the global nature of the flow field.

Figure 9 is a side view plot of the velocity vectors in the plane of symmetry of the jet for case D. Compared to Figure 6, it clearly shows that the solution has not changed in this region even though the local grid refinement has been increased. The velocity vectors indicate that the primary structure contains two counter-rotating vortices upstream of the jet, partitioned by the primary nodal point of attachment. Downstream of the nodal point and immediately upstream of the jet, the counter-clockwise vortex is reinforced by the jet stream. Ahead of the attachment point, the fluid which originated far upstream and immediately adjacent to the surface spirals into the primary clockwise vortex at the saddle point. The next layer of fluid similarly forms the forward-most secondary clockwise system. The rest of the entrained fluid develops into the secondary counter-clockwise rotating vortex beneath the two clockwise vortices and appears as the secondary separated flow region. Figure 10, which presents the comparison for the overall surface shear pattern for cases B and D, clearly shows that the location and extent of the secondary structure are identical for the two cases. The locations of the primary convergence lines for both cases agree within $\delta/10$,
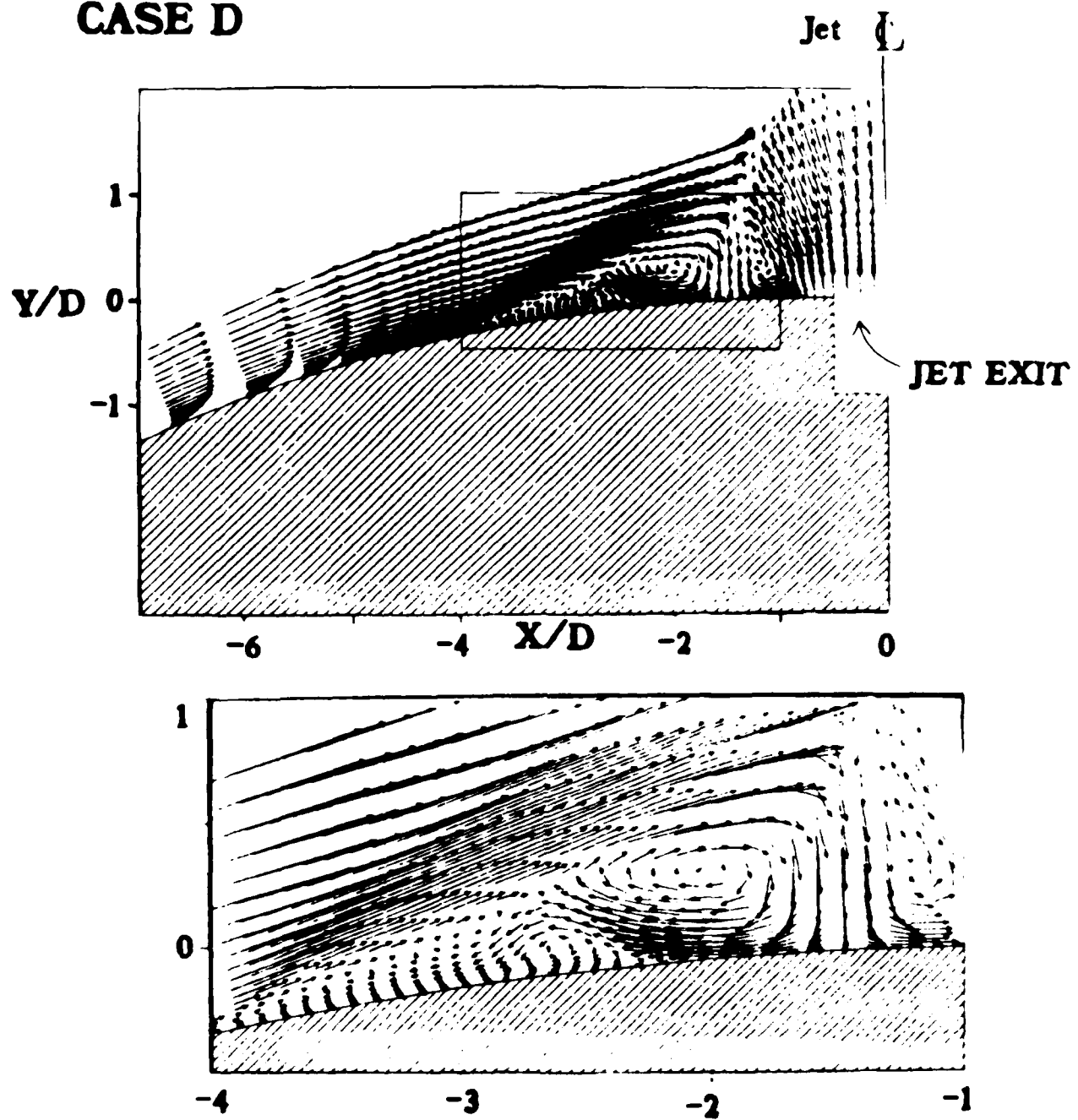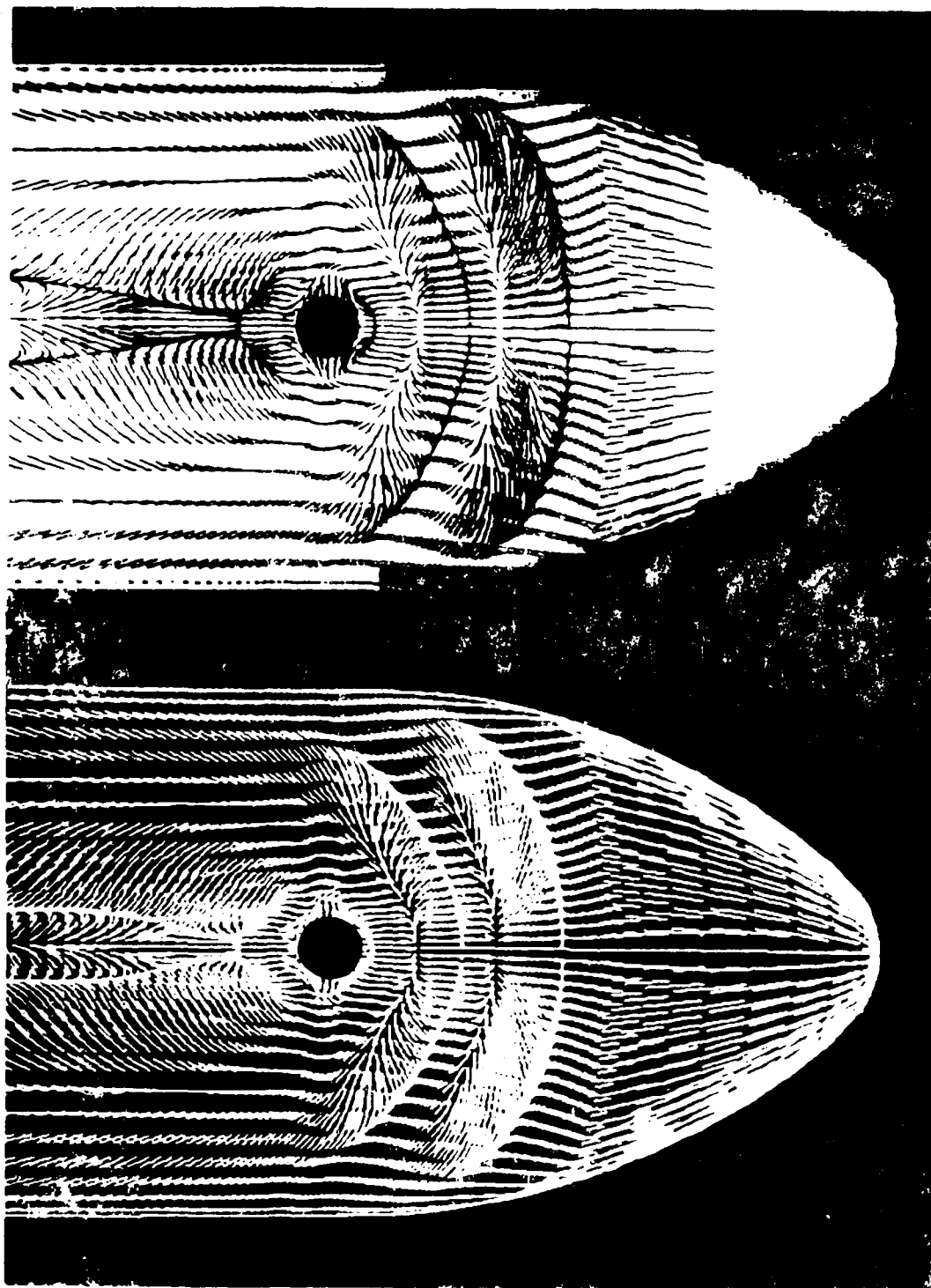
Figure 9. Velocity Vectors in the Plane of Symmetry

19

CASE B

CASE D

Figure 10. Comparison of Shear Flow ...

and the remaining convergent and divergent limiting surface streamlines show even closer agreement. The overall structure of the shear pattern remains invariant upstream of the jet, with no new topological singularities observed. Thus, for this region, the solution is now grid independent, and the solution of case B stands as representative of the complex interaction structure.

SECTION III

ROTATION STUDY

1. ANALYSIS

When the equation of fluid motion is expressed in the rotating frame of reference, the fictitious Coriolis and centrifugal forces must be explicitly included in the formulation. The Rossby number, $U/L\Omega$, a convenient measure of the ratio of inertial and Coriolis forces, becomes an additional dynamic similarity parameter for rotating flow systems (Reference 26). For a typical hypersonic aerodynamic configuration requiring spinning motion to maintain stability, the Rossby number is around 750. This Rossby number was simulated for the investigated configuration by rotation at an angular velocity Ω of 30 radians per second. The solution obtained at this Rossby number will be termed case E. In order to determine the influence of the Coriolis force on the pattern of the flow field, solutions were also obtained at Rossby numbers of 75 (case F) and 7.5 (case G), spanning a range of three decades.

Grid A was chosen for the rotation study, since it offered a reasonably accurate solution of global flow field features at a minimum expenditure of computer resources. The numerical algorithm used for the rotation study was identical to the one used in the grid refinement study. The governing equations and

the numerical boundary conditions were altered (as follows) to take into account the apparent Coriolis and centrifugal accellerations in the rotating frame of reference. The Navier-Stokes equations can be written in the flux vector form as

$$\frac{\partial U}{\partial t} + \frac{\partial F}{\partial x} + \frac{\partial H}{\partial y} + \frac{\partial G}{\partial z} = 0 \ , \tag{1}$$

where

$$U = \begin{bmatrix} \rho \\ \rho u \\ \rho v \\ \rho w \\ \rho e \end{bmatrix}$$

$$F = \begin{bmatrix} \rho u \\ \rho u^2 + \tau_{xx} \\ \rho uv + \tau_{xy} \\ \rho uw + \tau_{xz} \\ (\rho e + \tau_{xx})u + \tau_{xy}v + \tau_{zx}w - k\frac{\partial T}{\partial x} \end{bmatrix}$$

$$G = \begin{bmatrix} \rho v \\ \rho uv + \tau_{xy} \\ \rho v^2 + \tau_{yy} \\ \rho vw + \tau_{yz} \\ (\rho e + \tau_{yy})v + \tau_{yx}u + \tau_{yz}w - k\frac{\partial T}{\partial y} \end{bmatrix}$$

$$H = \begin{bmatrix} \rho w \\ \rho uw + \tau_{xz} \\ \rho vw + \tau_{yz} \\ \rho w^2 + \tau_{zz} \\ (\rho e + \tau_{zz})w + \tau_{xz}u + \tau_{yz}v - k\frac{\partial T}{\partial z} \end{bmatrix}$$

When the above equations are written in terms of the relative velocity in the rotating frame of reference, the basic form of the equations remains invariant. The additional acceleration terms in the rotating frame are accounted for by

adding source terms to four of the five equations. This is written in vector form as:

$$\frac{\partial U}{\partial t} + \frac{\partial F}{\partial x} + \frac{\partial G}{\partial y} + \frac{\partial H}{\partial z} = S ,$$ (2)

where

$$S = \begin{bmatrix} 0 \\ -\rho [2\bar{\Omega}x\bar{u} + \bar{\Omega} \times (\bar{\Omega}x\bar{r})]_i\text{th component} \\ -\rho [2\bar{\Omega}x\bar{u} + \bar{\Omega} \times (\bar{\Omega}x\bar{r})]_j\text{th component} \\ -\rho [2\bar{\Omega}x\bar{u} + \bar{\Omega} \times (\bar{\Omega}x\bar{r})]_k\text{th component} \\ -\rho\bar{u} \cdot [\bar{\Omega}x(\bar{\Omega}x\bar{r})] \end{bmatrix}$$

When the rotational motion is restricted about the streamwise axis of the body ($\bar{\Omega} = \Omega\hat{i}$), the source vector has only three non-zero terms:

$$S = \begin{bmatrix} 0 \\ 0 \\ \rho\Omega^2 y + 2\rho\Omega w \\ \rho\Omega^2 z - 2\rho\Omega v \\ \rho\Omega^2 (vy + wz) \end{bmatrix}$$

It may be interesting to note that the Coriolis force has no contribution to the energy equation, since it is a force directed at right angles to both the axis of rotation and the local velocity vector. The implementation of boundary conditions at the solid surface must also be changed in the rotating frame. The compatibility condition at the surface can be satisfied by changing the normal $\Delta P_{wall} = 0$ to $\Delta P_{wall} = \rho\Omega^2 r\Delta r$, where ρ and r are evaluated at the body surface.

The relative impact of the Coriolis and centrifugal forces can be determined by computing and comparing their magnitudes

throughout the flow field. The centrifugal forces are linearly proportional to the radial distance from the axis of rotation, and their effect should become stronger in the outer region of the flow. The Coriolis forces, however, must reside where there are high velocity components normal to the axis of rotation. It follows that the strongest Coriolis force should occur as the jet issues from the body. Any small change in structure at this point should theoretically propagate and amplify downstream in the trajectory of the jet, so the jet trajectory may serve as the best indicator of the presence of significant Coriolis effects.

In the interaction region immediately upstream and downstream of the jet, velocities are small compared to other regions of the flow field, especially near the surface. The separated flow pattern is known to be sensitive to any small disturbances. We could expect that rotational forces might cause significant changes in the local structure. We will examine the local shear stress formations upstream and downstream of the jet for possible asymmetries.

2. DISCUSSION OF RESULTS

Figure 11 depicts a comparison of the relative magnitude of the maximum Coriolis and centrifugal forces for cases E, F, and G. The centrifugal force is three orders of magnitude weaker than the Coriolis force for case E, the lowest spinning rate simulated. Even at an angular velocity 100 times greater than the case of interest, the centrifugal force, which is propor-
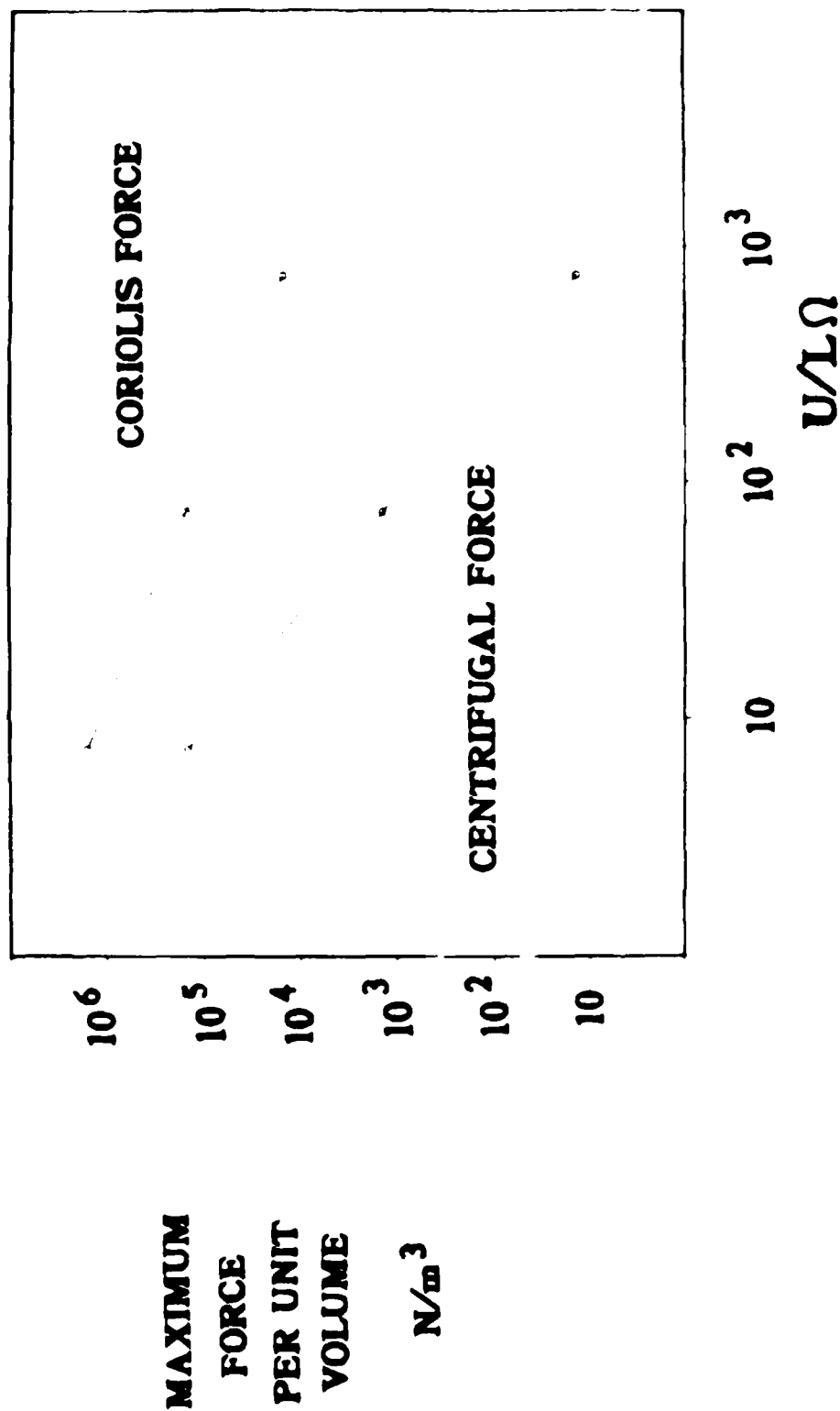
Figure 11. Magnitude of Maximum Coriolis and Centrifugal Forces vs. Rossby Number

tional to Ω^2, is an order of magnitude smaller than the Coriolis force. For all three cases studied, the centrifugal force probably has not substantially affected the formation of the flow field.

Figure 12 consists of two contour plots which show the magnitude of Coriolis force for sections of the entire flow field for case E. In the longitudinal plane of symmetry, the Coriolis forces are shown to be strongest at the jet exit, and negligible elsewhere. The contour levels exhibited in the figure represent the upper 90 percent values of the magnitudes of Coriolis force for the complete flow field. The cross-sectional contours taken at the jet location again show that the Coriolis forces are only significant near the jet exit.

Figure 13 compares the cross-sectional view of the Mach number contours at the jet location for cases A, E, F, and G. We see that case E, which satisfies the Rossby number similarity for a typical hypersonic configuration of practical interest, is identical to case A. Rotation at a rate 10 times higher than case E still yields no appreciable difference. It is only when the angular velocity is increased by two orders of magnitude over the rate of interest that a noticeable change in the shock structure takes place. In this case, the shock envelope immediately acquires an asymmetrical shape. The trajectory of the jet is disturbed only in case G, where it already has begun to shift away from the direction of rotation due to the restoring effect of the Coriolis force.
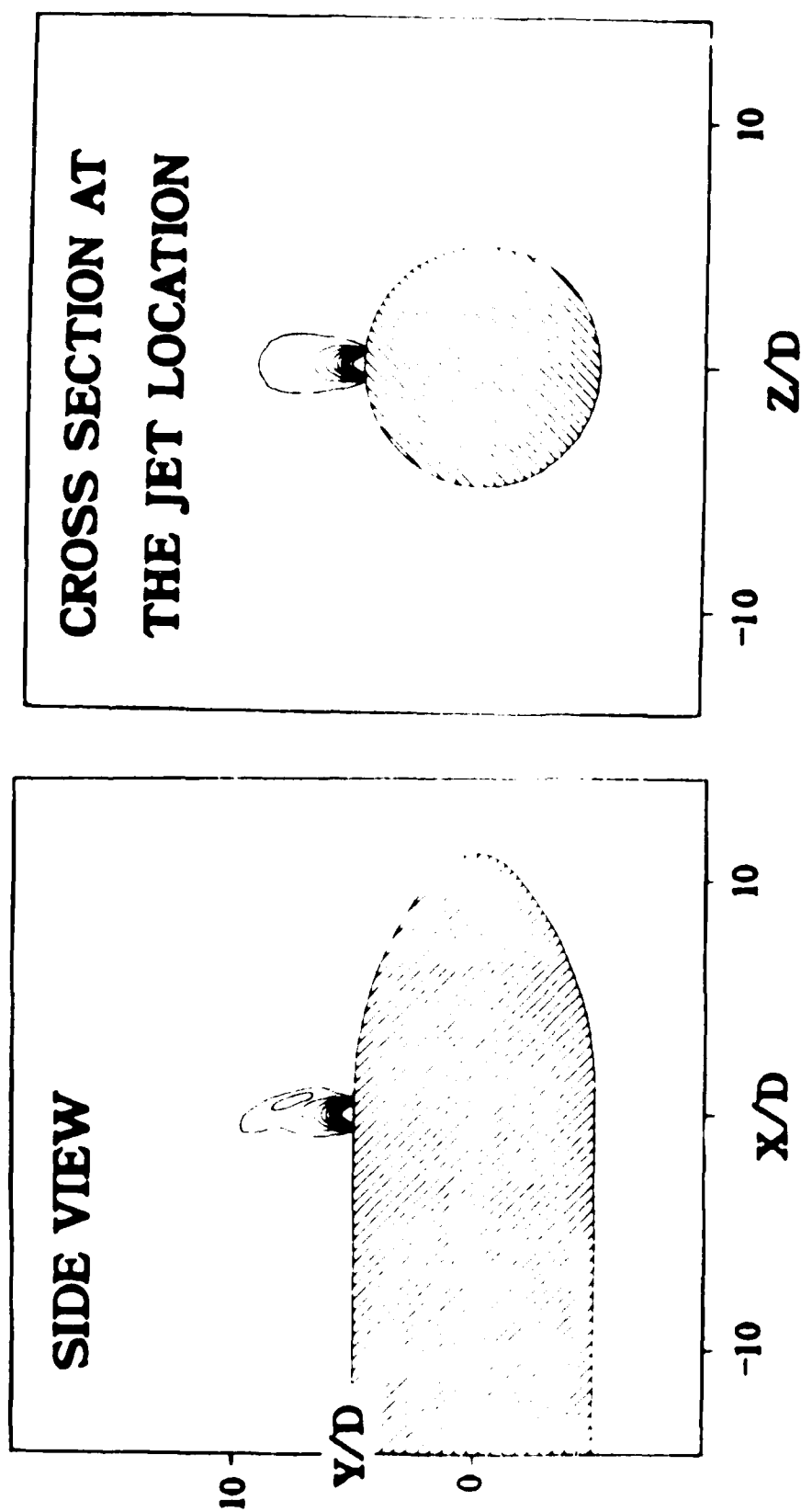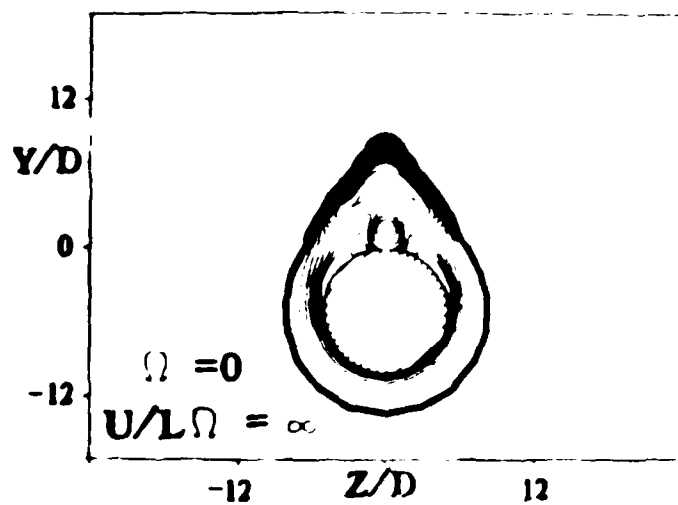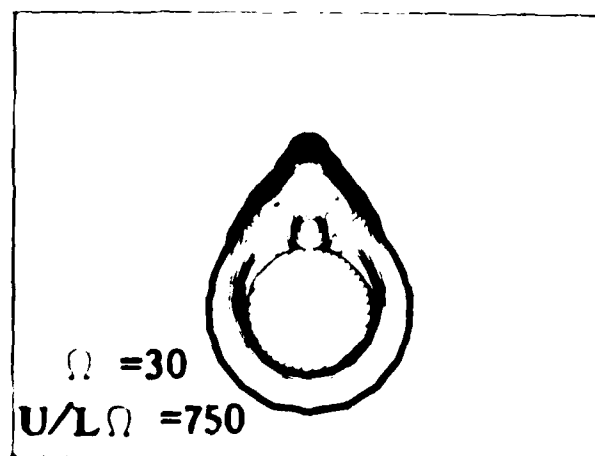
CROSS SECTION AT
THE JET LOCATION

SIDE VIEW

Figure 12. Region of Significant Coriolis Forces

U L = 750   = 80

CASE A

CASE E
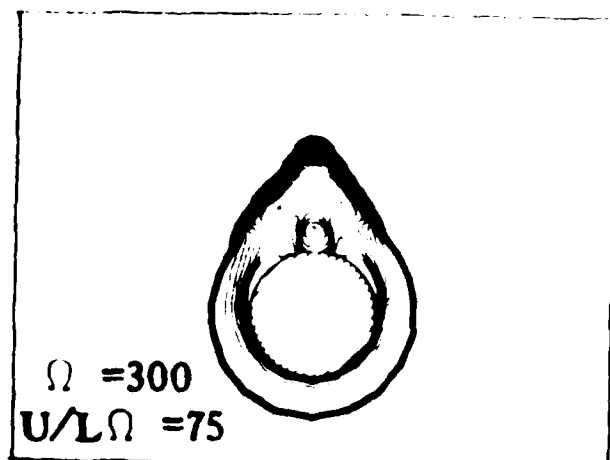
CASE F
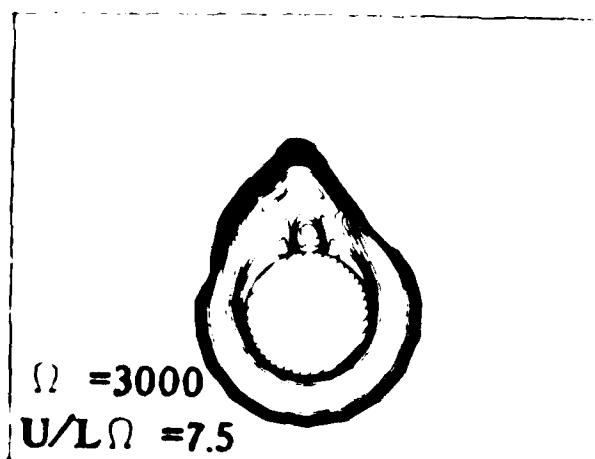
CASE G

Downstream of the jet, the effects due to rotation are consistent with previous findings. Since the most pronounced rotational effects occur at the jet exit, the jet plume should accentuate disturbance. Figures 14 and 15, which present Mach contours at stations six and twelve jet diameters downstream of the jet, support this observation. At the rotation rate that satisfies the similarity condition, no rotational effect can be observed on the flow field. Only at the highest rotation rate computed is there an appreciable change in the shock structure and jet trajectory. For this case, the disturbance originates at the jet exit and propagates downstream.

The behavior of the shear vectors is identical for all four cases in the near surface region upstream of the jet. This is not surprising in view of the computed magnitude of Coriolis forces outlined earlier. In the separated flow region upstream of the jet, there are no rotation forces with sufficient strength to alter the flow.

Results are slightly different downstream of the jet, however, as shown in Figure 16. The surface shear patterns are the same for cases A, E, and F, but case G begins to show some asymmetry due to rotation. The footprint of the jet wake is shifted slightly away from the direction of rotation, consistent with the shift in both the jet trajectory and the shock structure.

The existence of significant changes in the flow properties near the jet can be determined by examining the close up
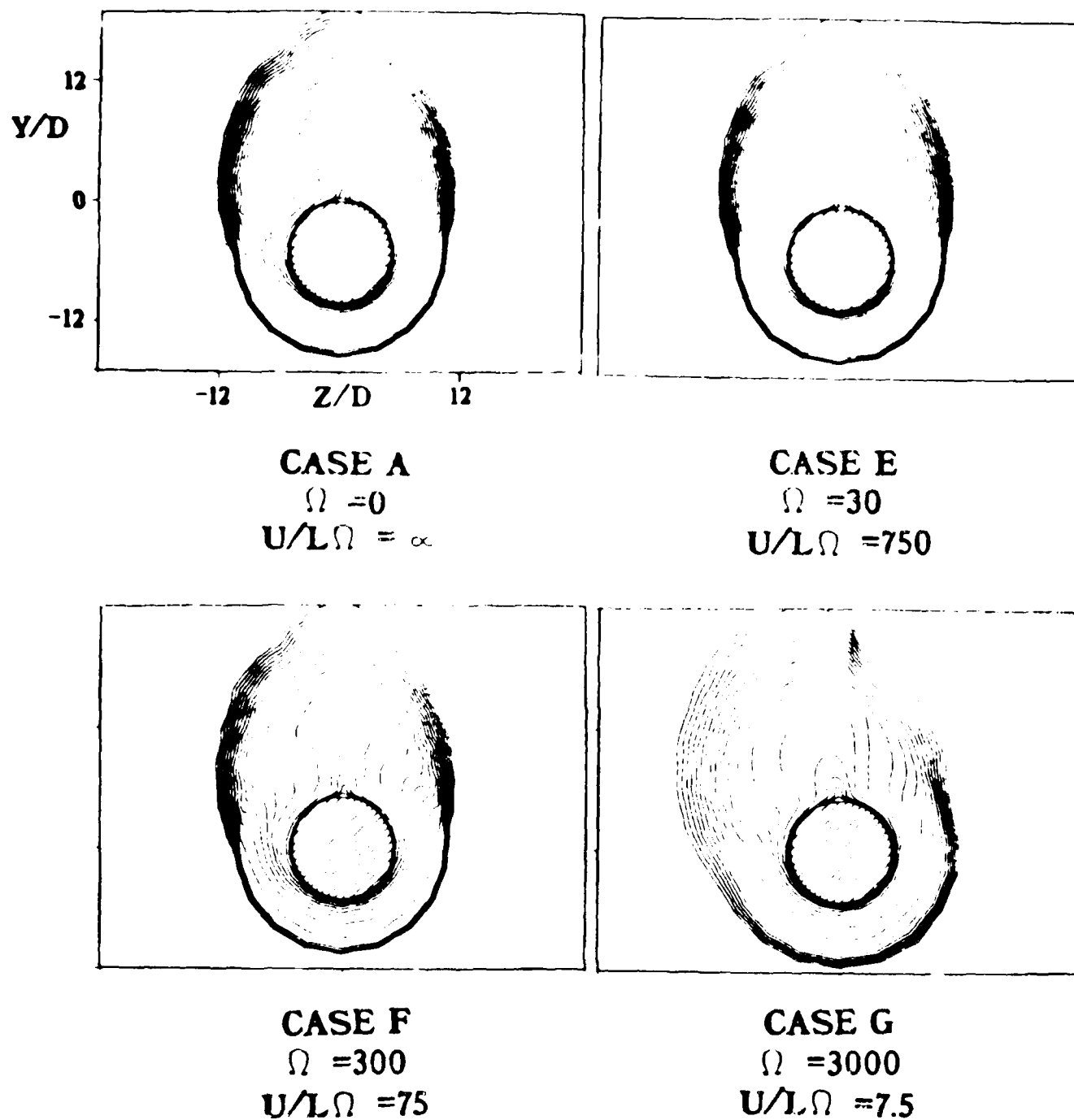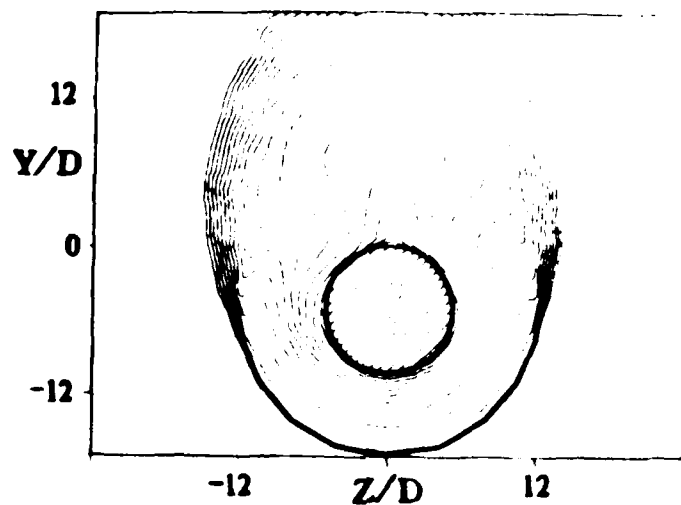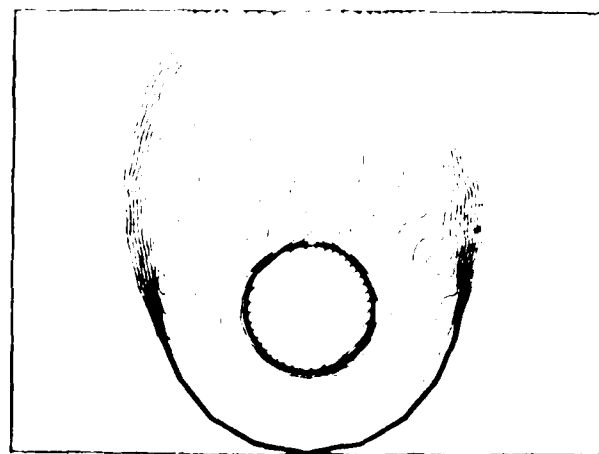
30

CASE A
$\Omega = 0$
$U/L\Omega = \infty$

CASE E
$\Omega = 30$
$U/L\Omega = 750$

CASE F
$\Omega = 300$
$U/L\Omega = 75$

CASE G
$\Omega = 3000$
$U/L\Omega = 7.5$

Figure 15. Mach Number Contours
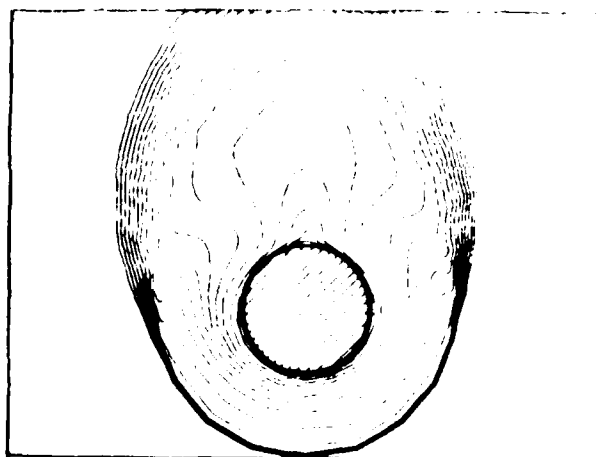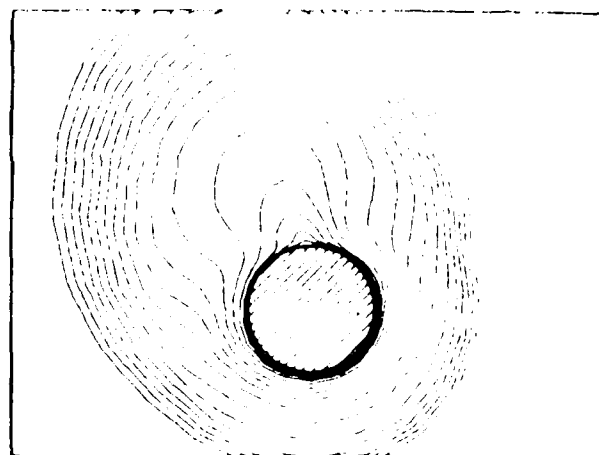
$X/D = 6$

31

CASE A
$\Omega = 0$
$U/L\Omega = \infty$

CASE E
$\Omega = 30$
$U/L\Omega = 750$

CASE F
$\Omega = 300$
$U/L\Omega = 75$

CASE G
$\Omega = 3000$
$U/L\Omega = 7.5$

Figure 16. Mach Number Contours

$X/D = 12$

Z/D

-2

2

0 2 X/D 6

CASE A
Ω =0
$U/L\Omega$ = ∞

CASE E
Ω =30
$U/L\Omega$ =750

CASE F
Ω =300
$U/L\Omega$ =75
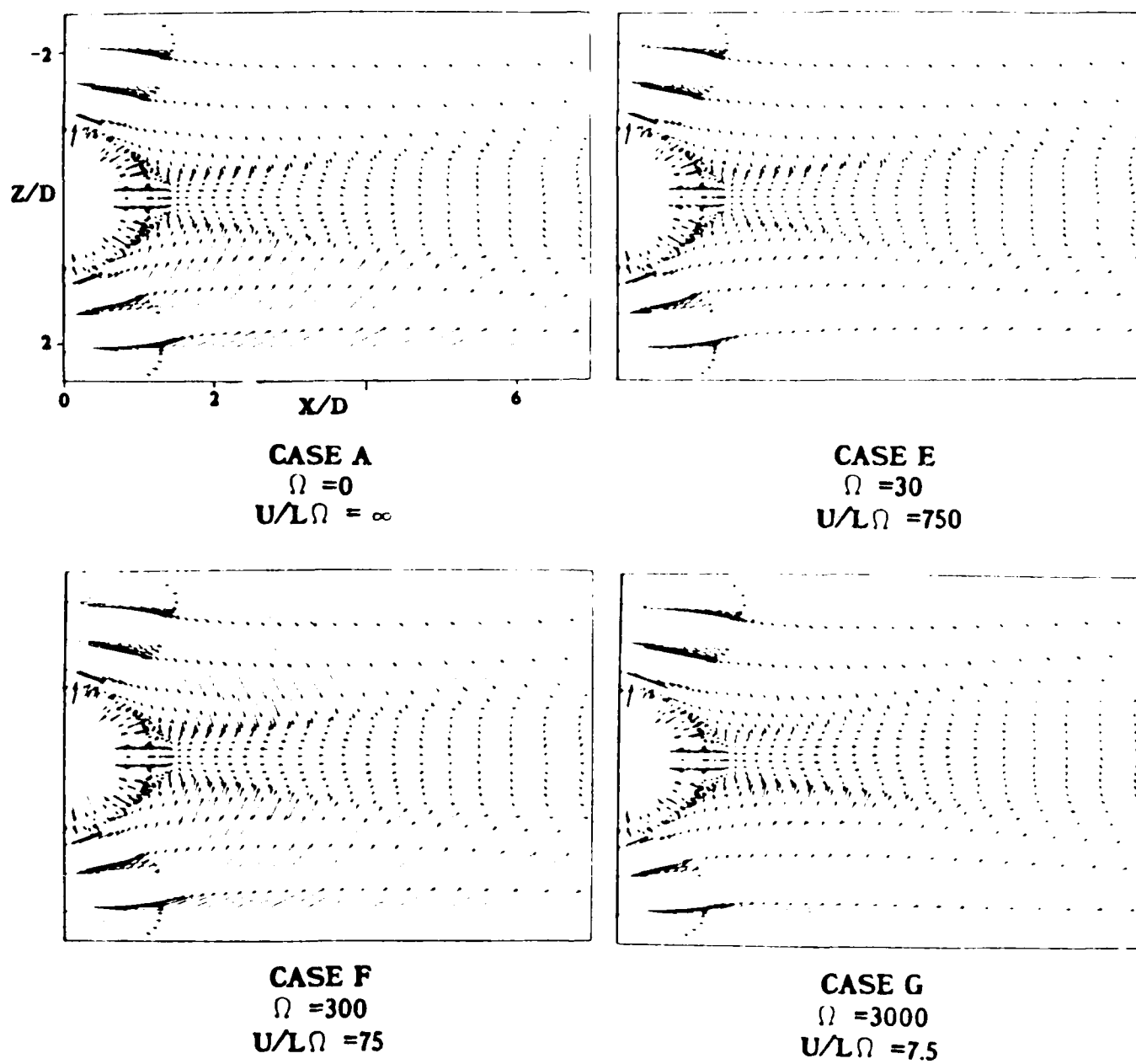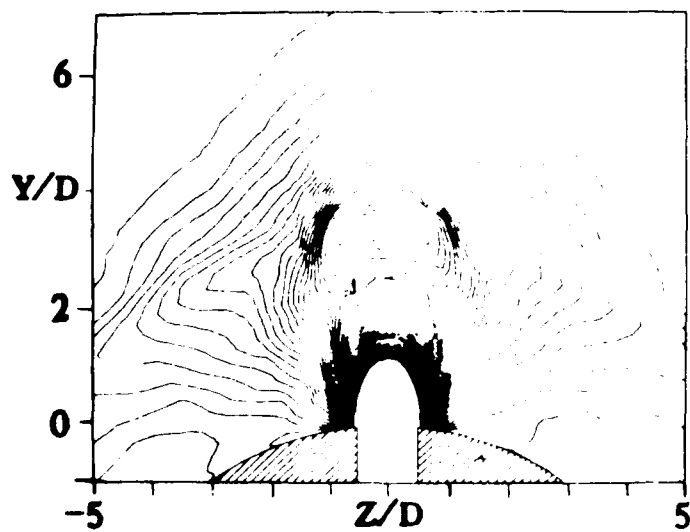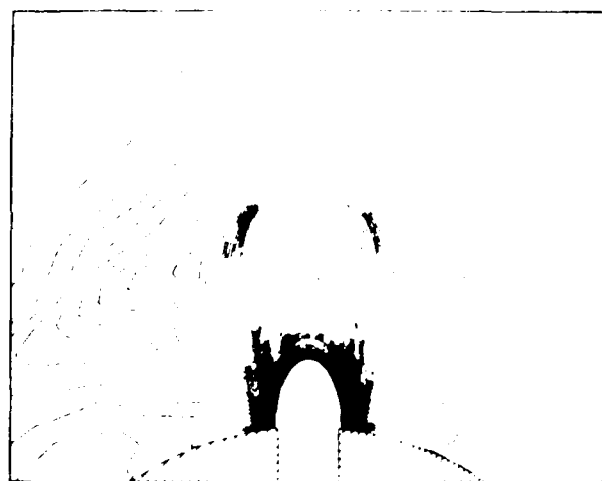
CASE G
Ω =3000
$U/L\Omega$ =7.5

Figure 16.   Surface Shear Vectors Downstream of Jet

behavior of fluid density in that region. Figure 17 shows the cross-sectional contour of density at the jet location in detail for cases A, E, F, and G. The contours for cases A, E, and F are identical within the range of numerical error. Case G, simulating the highest rate of rotation, shows large changes of the local flow field properties induced by the much higher rotation rate. The asymmetry of density contours in case G indicates a changes in trajectory of the jet due to the Coriolis forces. Note, however, that very near the jet exit the density contours retain the symmetric distribution.

Figure 18 shows the side view of the plane of symmetry of the jet for cases A, E, F, and G. Here, no changes are noted in the flow properties near the jet for any of the computed results. This observation was anticipated and used as a benchmark for the present investigation. Since the centrifugal force is negligible in comparison with the Coriolis force and the latter must be directed at right angles to both the axis of rotation and the jet velocity, the rotational forces must be exerted only in the circumferential direction. The effect of rotation projected in the plane of symmetry of the jet is neither expected nor generated numerically for the cases under consideration.
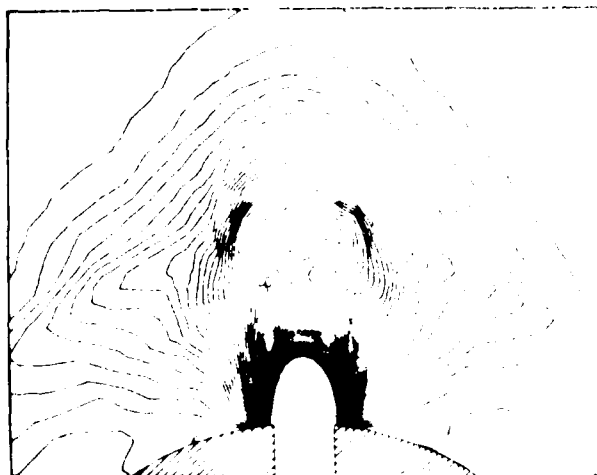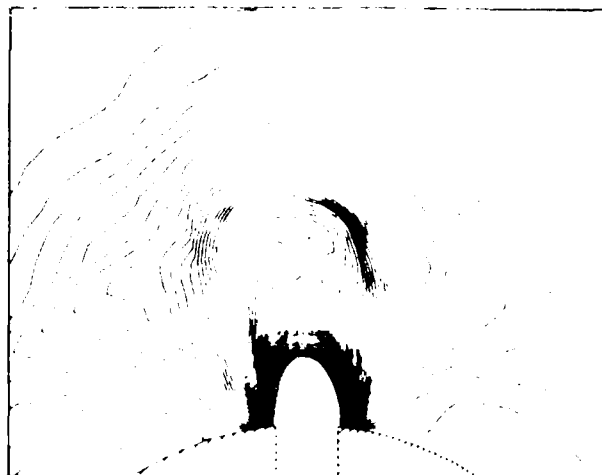
Figure 17. Density Contours at the Jet Cross Section
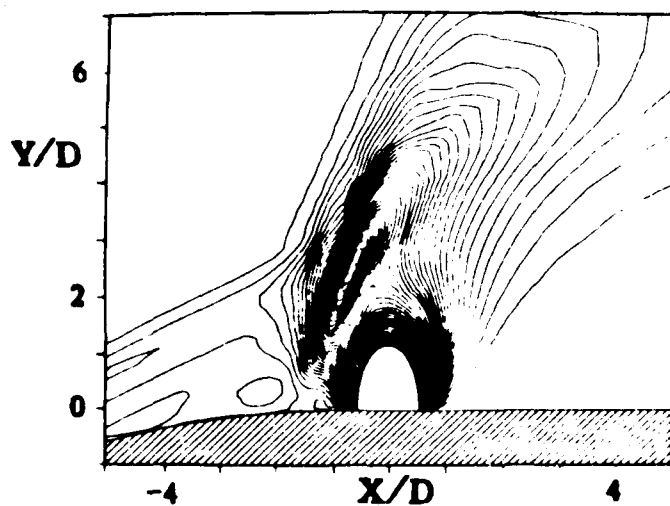
CASE A
$\Omega = 0$
$U/L\Omega = \infty$

CASE E
$\Omega = 30$
$U/L\Omega = 750$

CASE F
$\Omega = 300$
$U/L\Omega = 75$

CASE G
$\Omega = 3000$
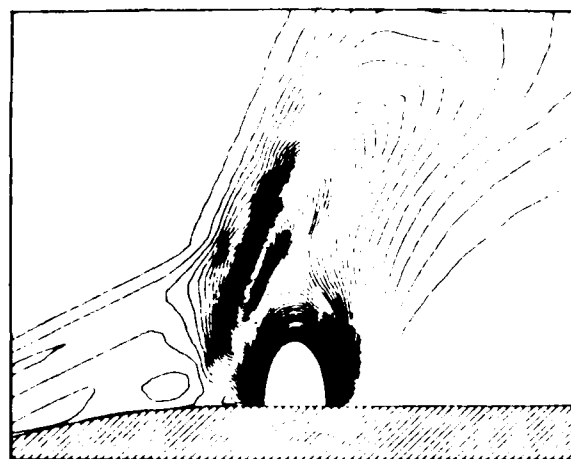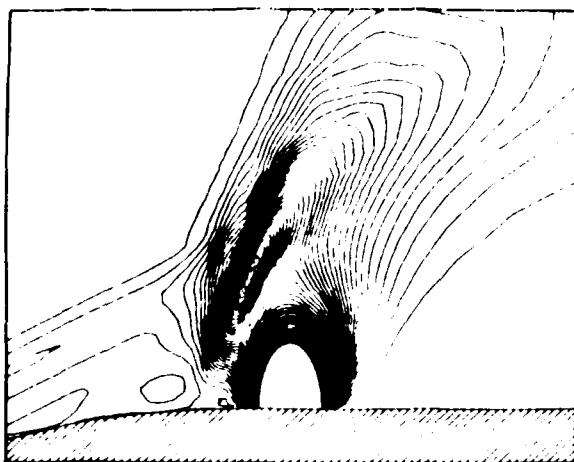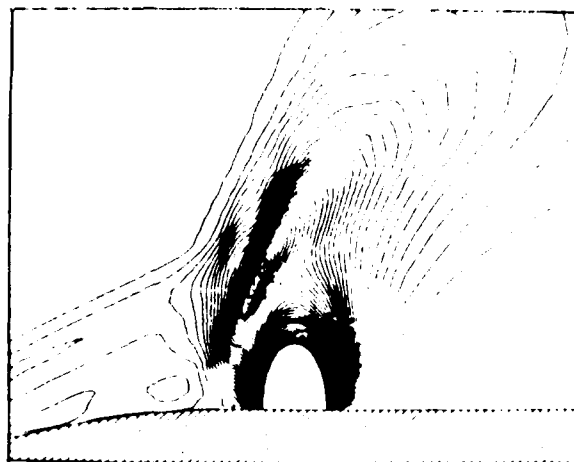$U/L\Omega = 7.5$

Figure 18. Side View of Density Contours in the Jet Plane of Symmetry

SECTION IV

CONCLUSIONS

Flow fields of a supersonic jet ejected from an ogive cylinder into a hypersonic freestream with and without rotating motion have been numerically simulated. For the non-rotating calculations, the three-dimensional separated flow, consisting of two pairs of counter-rotating vortices, replicates experimental observations. Even though the definition of the resultant shock wave is smeared by the shock capturing scheme, the computed complex vortical structure upstream of the jet is accurate and independent of further mesh system refinement.

The rotating flow system was computed in a rotating frame of reference. Three different body rotation rates corresponding to a range of Rossby numbers of 750, 75, and 7.5 were examined. At the highest Rossby number corresponding to the dynamic condition of practical engineering interest, the flow field in the rotating frame of reference is identical to that in the non-rotating case. The entire flow formation rotates as a solid bulk. The jet plume and the downstream shock wave envelope exhibit a circumferential shift due to the body rotation only at the lowest Rossby number examined, 7.5.

REFERENCES

1. Keffer, J. F. and Baines, W. D., "The Round Turbulent Jet in a Cross-Wind," Journal of Fluid Mechanics, Vol. 15, 1963, pp. 481-496.

2. Kamotani, Y. and Greber, I., "Experiments on a Turbulent Jet in a Cross Flow," AIAA Journal, Vol. 10, No. 11, November 1972, pp. 1425-1429.

3. Adler, D. and Baron, A., "Prediction of a Three-Dimensional Circular Turbulent Jet in Crossflow," AIAA Journal, Vol. 17, No. 2, February 1979, pp. 168-174.

4. Durando, N. A., "Vortices Induced in a Jet by a Subsonic Cross Flow," AIAA Journal, Vol. 9, No. 2, February 1971, pp. 325-327.

5. Sykes, R. I., Lewellen, W. S., and Parker, S. F., "On the Vorticity Dynamics of a Turbulent Jet in a Crossflow," Journal of Fluid Mechanics, Vol. 168, 1986, pp. 393-413.

6. Demuren, A. O., "Encyclopedia of Fluid Mechanics," (ed Cheremisinoff, N. P.), Blank Press, 1985, Volume 2, pp. 430-465.

7. Chien, J. C. and Schetz, J. A., "Numerical Solution of the Three-Dimensional Navier-Stokes Equations with Application to Channel Flows and a Buoyant Jet in a Cross Flow," ASME, Journal of Applied Mechanics, Vol. 42, September 1975, pp. 575-579.

REFERENCES

(Continued)

8. Zukoski, E. E. and Spaid, F. W., "Secondary Injection of Gases into a Supersonic Flow," AIAA Journal, Vol. 2, No. 10, October 1964, pp. 1689-1696.

9. Manela, J. and Seginer, A., "Jet Penetration Height in Transonic Flow," AIAA Journal, Vol. 24, No. 1, January 1986, pp. 67-73.

10. Broadwell, J. E. and Breidenthal, R. E., "Structure and Mixing of a Transverse Jet in Incompressible Flow," Journal of Fluid Mechanics, Vol. 148, 1984, pp. 405-412.

11. Zubkov, A. I. and Glagolev, A. I., "The Effect of Boundary Layer Thickness and Transverse Curvature of the Surface on the Geometry and Forces Acting in the Separation Zone Produced by Injection of a Jet into a Supersonic Flow Over That Surface," Fluid Mechanics - Soviet Research, Vol. 8, No. 1, January-February 1979, pp. 69-79.

12. McMahon, H. M. and Mosher, D. K., "Experimental Investigation of Pressures Induced on a Flat Plate by a Jet Issuing into a Subsonic Crosswind," NASA SP-218, Paper 4, 1969.

13. Shang, J. S., McMaster, D. L., Scaggs, N., and Buck, M., "Interaction of Jet in Hypersonic Cross Stream," AIAA Paper 87-0055, January 1987.

14. Avduevskii, V. S., Medvedev, K. I., and Polyanskii, M. N., "Interaction of a Supersonic Flow with a Transverse Jet

REFERENCES

(Continued)

Injected Through a Circular Aperture in a Plate," Izvestiya
Akademii Nauk SSSR, Mekhanika Zhidkosti i Gaza, No. 5, 1970,
pp. 193-197.

15. Glagolev, A. I., Zubkov, A. I., and Panov, Yu. A.,
"Supersonic Flow Past a Gas Jet Obstacle Emerging from a
Plate," Izvestiya Akademii Nauk SSSR, Mekhanika Zhidkosti i
Gaza, No. 3, 1967, pp. 97-102.

16. Baker, A. J., Snyder, P. K., and Orzechowski, J. A.,
"Three-Dimensional Nearfield Characterization of a VSTOL Jet in
Turbulent Crossflow," AIAA Paper 87-0051, January 1987.

17. Peake, D. J. and Tobak, M., "Three-Dimensional Interactions
and Vortical Flows with Emphasis on High Speeds," AGARD-AG-252,
July 1980.

18. Settles, G. S. and Dolling, D. S., "Swept Shock
Wave/Boundary-Layer Interactions," AIAA Progress in
Astronautics and Aeronautics, Tactical Missile Aerodynamics,
ed M. Hemsch and J. Nielsen, 1986.

19. Lighthill, M. J., "Laminar Boundary Layers," (ed. L.
Rosenhead), Oxford University Press, 1963, pp. 72-82.

20. Hunt J. C. R., Abell, C. J., Peterka, J. A., and Woo, H.,
"Kinematical Studies of the Flows Around Free or Surface-
Mounted Obstacles; Applying Topology to Flow Visualization,"
Journal of Fluid Mechanics, Vol. 86, 1978, pp. 179-200.

REFERENCES

(Concluded)

21. Tobak, M. and Peake, D. J., "Topology of Three-Dimensional Separated Flows," Annual Review of Fluid Mechanics, 1982, pp. 61-85.

22. Linton, S. W. and Shang, J. S., "A Numerical Simulation of Jet Impingement Cooling in a Rotating Frame of Reference," AIAA Paper 87-0609, January 1987.

23. Hung, C.-M. and Buning, P. G., "Simulation of Blunt-Fin-Induced Shock-Wave and Turbulent Boundary-Layer Interaction," Journal of Fluid Mechanics, Vol. 154, 1985, pp. 163-185.

24. Baldwin, B. and Lomax, H., "Thin Layer Approximation and Algebraic Model for Separated Turbulent Flows," AIAA Paper 78-257, January 1978.

25. MacCormack, R. W., "The Effect of Viscosity in Hypervelocity Impact Cratering," AIAA Paper 69-354, January 1969.

26. Batchelor, G. K., "An Introduction to Fluid Dynamics," Cambridge University Press, 1967, pp. 555-557.

LIST OF SYMBOLS

D   diameter of jet aperture

e   total energy per unit mass

F,G,H   flux vectors defined by equation 1

k   thermal conductivity

L   characteristic length

M   Mach number

P   pressure

P_t pitot tube pressure

r   radial distance from the axis of symmetry

R   radius of cylinder

Rey   Reynolds number

S   rotational source vector defined by equation 2

t   time

T   temperature

u,v,w   velocity components in the Cartesian frame

$\vec{u}$ velocity vector

x,y,z   coordinates in the Cartesian frame

δ boundary layer thickness

ρ fluid density

$\tilde{\tau}$ stress tensor

$\vec{\Omega}$ angular velocity, radians per second

Subscript

i,j,k   unit vector in the Cartesian frame

LIST OF SYMBOLS

(Concluded)

j   denotes condition of jet

o   denotes stagnation condition

∞   denotes freestream conditions

END

DATE

FILMED

MARCH

1988

DTIC